Synthesis of Al doped ZnO nanoparticles by aqueous coprecipitation

Fabien Giovannelli, Alphonsine Ngo Ndimba, Pablo Diaz-Chao, Mikael Motelica-Heino, P.I. Raynal, Cecile Autret, Fabian Delorme

Synthesis of Al doped ZnO nanoparticles by aqueous coprecipitation

F. Giovannelli[*1], A. Ngo Ndimba[1], P. Diaz-Chao[2], M. Motelica-Heino[3], P.I. Raynal[4], C. Autret[1], F. Delorme[1]

[1] *Université François Rabelais de Tours, CNRS, CEA, INSA, GREMAN UMR 7347, IUT de Blois, 15 rue de la chocolaterie, CS 2903, 41029 Blois Cedex, France.*

[2]*CRISMAT, UCBN, ENSICAEN, 6 Boulevard du Maréchal Juin, 14050 Caen cedex, France*

[3]*Université d'Orléans CNRS/INSU Institut des Sciences de la Terre d'Orléans, UMR 7327 Campus Géosciences 1A, rue de la Férollerie 45071 Orléans cedex 2, France.*

[4]*Plateformes des Microscopies-Université François Rabelais et CHRU de Tours, 10 boulevard Tonnellé, 37032 Tours cedex, France*

[*] : corresponding author. Tel. : +33-2-54-55-21-10 ; E-mail : fabien.giovannelli@univ-tours.fr.

Abstract

Al-doped ZnO particles were obtained by a simple route: soda addition in aqueous cationnic solution. The effects of temperature, hydrolysis duration, reagent concentration and time were investigated. A non-topotactic reaction mechanism, involving firstly the precipitation of various hydroxide compounds depending on the route (low or high pH), followed by the dissolution-recrystallization of the hydroxide species into ZnO was demonstrated. The Al concentration in the final ZnO nanopowders did not exceed 0.3 at% which correspond to the solubility limit of Al in ZnO. The different experimental conditions allow the morphology of ZnO particles to be controlled from isotropic nanoparticles of several tens of nanometers, platelets of several hundreds of nanometers or agglomerates of needle like particles.

Introduction

ZnO has focused much attention for electronic and optoelectronic applications as a large band gap material [1-3]. In order to manufacture ZnO-based optoelectronic devices,both n- and p-type ZnO are needed. It is easy to obtain good conductive n-type ZnO by mono-doping III group elements as donors. Al doped n-type ZnO, in particular, exibits high electrical conductivity and optical transparency in the visible region. It is a transparent conductive oxide which could replace the more expensive indium tin oxide [4-7]. Morever the Al doped ZnO is also highly promising as a potential high-temperature thermoelectric material [8-10].

Moreover, among inorganic semiconductors, reported morphologies of ZnO are the richest. Indeed, a wide variety of ZnO micro/nano-structures including wires, rods, belts, tubes, cages, rings or flowers have been synthesized by many methods, such as sol-gel processing, vapor deposition, hydrothermal syntesis, thermal decomposition or microwave synthesis [11-16]. Precipitation from colloidal solutions is an usual method for producing transition metal oxide nanoparticles [17-19]. Two reactions are generally used to describe the precipitation process: Hydrolysis and water condensation. Hydrolysis consists in the formation of an insoluble hydroxide which can be converted into the oxide compound by heat assisted dehydratation. Indeed, in order to obtain ZnO, many studies used a thermal treatment after the precipitation step [20-23]. However, the water condensation phenomenom could also appear directly in the solution. ZnO precipitation in a solution heated to 80°C has been already reported [24-27]. Oliveira et al. [28] have proposed a precipitation under double-jet conditions to produce micrometric ZnO particles at room temperature. Moreover, recently, Yang et al. [29] have reported the obtention of ZnO at 25°C by adding soda to a Zn sulfate solution. However, in many applications ZnO doping is necessary in order to reach the best properties, especially Al doping.

In this study, the influence of different parameters (temperature, hydrolysis duration, reagent concentration and time) on the precipitation of Al-doped ZnO was studied as well as the reaction mechanisms.

Materials and methods

100 ml of cationic solution was obtained by dissolving $Zn(NO_3)_2,6H_2O$ (Aldrich 99.99%) and $AlCl_3$ (Acros 99%) in demineralized water. The concentration of Zn is 0.1M and Al concentration corresponds to 2 at% of Zn one. Precipitation was made by the dropwise addition of 125ml of NaOH solution at 1 mol/l (NaOH solid from Scharlau (99%)) during 25 minutes. The precipitate obtained was centrifuged at 4000 rpm during 5 min and washed with demineralized water. This step was repeated five times. The solid was finally dried at 80°C. The following synthesis parameters were modified: influence of reactant concentration (0.5M and 1M), Zn/OH molar ratio (0.1, 0.2 and 0.6), soda addition time (10 s) and temperature (25 °C and 60°C).

The morphologies of ZnO powders were analyzed on a ZEISS Ultra Plus field-emission scanning electron microscope (FE-SEM) operated at an acceleration voltage of 2 kV. The samples were platinum-coated prior to observation using a GATAN Precision Etching and Coating System (PECS™). Transmission electron microscopy samples were prepared by adding the powder to n-butanol and the small crystallites in suspension were deposited on a holey carbon film, supported by a copper grid. The electron diffraction and the high resolution electron microscopy were carried out with a JEOL 2100F electron microscope equipped with a tilting and rotating goniometer (200 kV and point resolution of 1.8 Å) and coupled with EDX analysis (Oxford).

Powder X-ray diffraction (XRD) patterns were acquired on a Bruker D8-Advance diffractometer in Bragg/Brentano geometry using Cu-K_α radiation and operating at 40kV and 40 mA at room temperature. Scans were recorded from 5° to 85° (2θ) with a step of 0.02 and a counting time of 1s per step.

Laser ablation–inductively coupled plasma–mass spectrometer (LA-ICP-MS) analysis was made on the samples. An element XR Thermo (Thermo Finnigan) ICP-MS, following the procedure described in previous studies [30-32] was used in combination with a VG UV laser probe, laser ablation sampling device. Solid samples were prepared as pressed pellets. Powder samples of 350 mg were put under a pressure of 8 metric tons, without added binder, to form 13 mm (diameter) x 1 mm (height) pellets. The repetition rate of the 266 nm wavelength laser was fixed to 10 Hz. Calibration took place with a certified artificial glass, NIST-610. Measurements were replicated four times to validate the analytical precision of the technique.

Results and discussion

When NaOH is added to the zinc solution, as described in the materials and methods section, the evolution of pH exhibits both important variations from pH 3 to 6 and then from pH 6.5 to 10.5. The solid precipitation appears with the first soda addition. The colour of the final solid precipitate is white. The final pH is higher than 12. The XRD pattern of the resulting powder exhibits all the peaks of ZnO (PDF card 01-070-8070) (Figure 1). However, the peak intensity of (002) planes is enhanced compared to the PDF card (01-070-8070). The SEM observations show the presence of two kinds of particles (Figure 2A): on the one hand, nanoparticles exhibiting an isotropic shape of several tens of nanometers and on the other hand, platelets like particles with a size of several hundreds of nanometers and a thickness of several tens of nanometers. The (002) peak intensity enhancement could be linked to the presence of these platelets in the powder. The analysis of Al concentration leads to a content of 0.1 at% which is far less than the initial content of 2 at. %.

Hydrolysis and water condensation depend on the reactant's concentrations and on the ratio Zn/OH. The influence of Zn concentration was evaluated by increasing the 0.1M initial concentration to 0.5 M and 1 M without changing the ratio Zn/OH=0.2 and the initial aluminum atomic percent. The XRD pattern of the 1 M sample only exhibits peaks related to ZnO (Figure 1). SEM observations still show the presence of the two kinds of particles (Figure 2B). However, the number of platelets increases. The analysis of Al concentration leads to a content of 0.28 at%. So the increase of the initial Zn concentration leads to an increase of the Al content in ZnO powder. This value is close to 0.3 at% which is the limit of solubility of Al in ZnO [33, 34]. Moreover, TEM analyzes analysis confirms these results, showing homogeneous compositions of the particles (Al concentrations close to 0.3 at %) regardless of their morphology. The 0.5M sample presents a similar behavior: XRD pattern only exhibits peaks related to ZnO and SEM observations show the presence of the two particle morphologies. The comparison of XRD data show that the full width at half maximum (FWHM) of all the peaks of the 0.1 M sample is larger than for the two other concentrations (Figure 1). This is consistent with SEM images, which show that in this case, the proportion of small particles is greater (Figure 2A). Therefore, the increase of the initial Zn concentration leads to a coarsening of particles and an increase in the aluminum content within the particles.

In order to observe its influence, the initial Zn/OH ratio (Zn/OH = 0.2) was initially decreased to 0.1 with an initial Zn concentration of 1 M. No significant difference was observed (Figure 3). Afterwards the ratio Zn/OH was increased to 0.6. The final pH was 7.9. In this final case, new peaks appeared on the XRD pattern which could be attributed to different phases (Figure 3) : zinc hydroxide salts structures (PDF-00-24-1460 and PDF 00-052-0627), $Al(OH)_3$ gibbsite (PDF-00-054-0036) and a Zn-Al hydrotalcite-like structure (PDF 00-057-0528) (Figure 3). These phases are layered hydroxides which are closely related to the brucite

structure [35-37]. The brucite structure is based on CdI_2 layers: divalent metal cations occupy the centers of OH^- octahedra joined by their edges to form infinite layers. The layers are held each other by weak intermolecular forces or hydrogen bondings. In this case of a hydrotalcite like structure, the substitution of a divalent cation by a trivalent cation in brucite structure induces the presence of an interlayer anion in order to conserve the electroneutrality of the structure. Gibbsite presents a brucite structure with one third empty octahedral sites, as aluminum has an oxidation state of three. The zinc hydroxide nitrate structure is formed by brucite layers presenting one quarter empty octahedra. Tetrahedrally coordinated zinc atoms are located above and below the empty octahedra. These layered hydroxides can present several kinds of crystallographic structures. The first key parameter is the nature of the layers, whereas the second one is their stacking, which can generate different polytypes. Moreover, XRD patterns exhibit two more small peaks that are not identified at 13.3 and 16.3 °2θ (Figure 3). These small peaks could be related to another layered hydroxide due to the large variety of structures in the family [37]. The high Zn/OH ratio leads to the presence of hydroxide in the resulting powder. However, the maximum intensity peaks in XRD is due to ZnO. The final Al concentration in the powder is 6 at% which is three times more than the initial solution content. It means that all of the aluminum is in different solid phases and that Zn has not yet totally precipitated at this pH value. The amphoteric character of Al explains the fact that when the pH increases to 12 the Al bearing phases are dissolved and the final content of Al is close to the solubility limit of Al in ZnO. This is consistent with dissolution-crystallization of preexisting hydroxides in ZnO when the pH increases.

This is consistent with previous reports as hydroxide compounds have already been proposed by several authors as intermediary phases [38-41]. However, the type of anions present in the solution as well as the experimental procedure seem to strongly influence the intermediary phases. Indeed, Hosono et al. [38], in a non-basic solution route to prepare ZnO, described the

polymerization of zinc acetate in layered Zn hydroxide acetate which is then hydrolyzed in order to obtain ZnO, whereas by adding soda in aqueous Zn acetate solution, Caillaud et al. [39] observe the appearance of ε-$Zn(OH)_2$. Nevertheless, the transformation of a hydroxide phase in another hydroxide compound is possible: indeed, Zn hydroxy-nitrate in the presence of acetate or in basic medium leads to the formation of ε-$Zn(OH)_2$ [40, 41].

When the soda addition time in our experimental procedure was reduced to 10 seconds instead of 25 minutes, the XRD exhibited the presence of ZnO and ε-$Zn(OH)_2$ phases (Figure 4). The most intense peaks corresponded to ε-$Zn(OH)_2$. Moreover, the FWHM of ε-$Zn(OH)_2$ was smaller than ZnO one. This could be linked to different particles sizes. This interpretation is consistent with the SEM images which show the presence of two kinds of particles (Figure 5A): well crystallized micrometric particles of ε-$Zn(OH)_2$ and submicrometric agglomerate of needle like particles of ZnO. These experimental conditions lead to a formation of particles in a basic solution (final pH>12) whereas in the conventional method crystallization occurs from pH = 3 to 12. Yang et al. [29] have also obtained ε-$Zn(OH)_2$ when they added the cationic solution to the soda solution. In order to investigate the relationships between ZnO and ε-$Zn(OH)_2$, a part of the slurry was aged 24 hours under vigorous stirring. The resulting XRD pattern also exhibited ε-$Zn(OH)_2$ and ZnO peaks (Figure 4 B). However the relative intensities indicate that the presence of ZnO is greater. SEM images still show the well-defined micrometric particles and submicrometric agglomerates of needle like particles (Figure 5B). However, the surfaces of the well-defined micrometric particles appear degraded by small holes and the presence of needle like particles is more important which is consistent with XRD patterns. In these experimental conditions, the $Zn(OH)_2$ particles are transformed slowly into ZnO nanoparticles by a non topotactic reaction, i.e. dissolution-recrystallization. The way of mixing the cationic and soda solutions leads to different intermediary phases and

therefore ZnO nanoparticles with different morphologies and sizes. Even if the final product is pure ZnO, the careful selection of the synthesis process is a route to tune the particles size and morphology.

The effect of the Al content was also studied from pure ZnO samples up to 5 at % Al. Pure ZnO was obtained at room temperature. In the case of pure ZnO, the powder exhibits a sand rose morphology with micrometric size platelets (Figure 6A). With 5 at % of Al, the powder morphology was essentially formed by small isotropic particles close to 30 nanometers (Figure 6B). The measured aluminum content in the powder only reaches 0.3 atomic percent which is the limit of solubility of Al in ZnO [33-34]. The increase of initial aluminum content allows increasing the final aluminum content up to the solubility limit and also enables the nucleation centers of ZnO to increase leading to a drop in the number of large platelet like particles. Indeed, the trivalent aluminum cation precipitates at lower pH than divalent cation leading to amorphous aluminum hydroxide which acts as nucleation centers for ZnO when the pH reaches higher values [42-44].

Finally, the effect of temperature was also studied. The experiment was carried out at 60°C. The XRD pattern exhibited only the peaks of ZnO (Figure 7). It is worth noting that relative intensities of XRD pattern peaks are similar to ZnO PDF card whereas in all the other experiments peak intensity of (002) plane are enhanced compared to PDF card. SEM images show that this sample is only composed of isotropic nanoparticles of several tens of nanometers in size (Figure 8). Therefore, the enhanced peak intensity of (002) plane can be correlated to the presence of the platelets in the samples.

Conclusions

Al-doped ZnO nanoparticles were synthesized with a simple precipitation process. A non-topotactic reaction mechanism, involving firstly the precipitation of various hydroxide compounds depending on the route (low or high pH), followed by the dissolution-recrystallization of the hydroxide species into ZnO, was demonstrated. When the initial pH is low, different Zn hydroxide salts precipitate whereas when the initial pH is high, the intermediary hydroxide phase is $Zn(OH)_2$. The Al concentration in the final ZnO nanopowders does not exceed 0.3 at% which corresponds to the reported solubility limit of Al in ZnO. The different experimental conditions allow the morphology of ZnO particles to be controlled from isotropic nanoparticles of several tens of nanometers, platelets of several hundreds of nanometers or agglomerates of needle like particles.

References

[1] Ü. Özgür, Y.I. Alivov, C. Liu, A. Teke, M.A. Reshchikov, S. Doğan , V. Avrutin, S.-J.Cho , H. J. Morkoç, A comprehensive review of ZnO materials and devices, Appl. Phys. 98 (2005) 41301- 41404.

[2] S.J. Pearton , D.P. Norton , K. Ip, Y.W. Heo, T. Steiner , Recent progress in processing and properties of ZnO, Progress in Materials Science 50 (2005) 293–340

[3] C. Klingshirn, ZnO: Material, physics and applications, Chem. Phys. Chem. 8 (2007) 782-803

[4] T. MinamI, T. Yamamoto, and T. Miyata, Highly transparent and conductive rare earth doped ZnO thin films prepared by magnetron sputtering,Thin Solid Films 366(2000) 63-68.

[5] K. Lee, E. Kim, H. Kim, H. Kang, J. Song, Low temperature Al doped ZnO films on a flexible substrate by DC sputtering Phys. Status Solidi C 5 (2008) 3344-3347.

[6] D. J. Cohen, K. C. Ruthe, and S. A.Barnett, Transparent conducting $Zn_{1-x}Mg_xO$:(Al,In) thin films, J. Appl. Phys. 96 (2004) 459-467.

[7] W. Beyer, J. Hupkes, and H. Stiebig, Transparent conducting oxide films for thin film silicon photovoltaics, Thin Solid Films 516 (2007) 147-154.

[8] T.Tsubota, M.Ohtaki, K. Eguchi and H. Arai, Thermoelectric properties of Al-doped ZnO as a promising oxide material for high temperature thermoelectric conversion, J. Mater. Chem. 7 (1997) 85–90.

[9] P. Jood, R. Mehta, Y. Zhang, G. Peleckis, X. Wang, R. W. Siegel, T. Borca-Tasciuc, S. Dou, G. Ramanath, Al-doped zinc oxide nanocomposites with enhanced thermoelectric properties, Nano Lett. 11 (2011) 4337–4342.

[10] E. Guilmeau, A. Maignan, C. Martin, Thermoelectric Oxides: Effect of Doping in Delafossites and Zinc Oxide, Journal of Electronic Materials 38 (2009) 1104-1108.

[11] Wang Z. L., ZnO nanowire and nanobelt platform for nanotechnology, Materials Science and Engineering R 64 (2009) 33–71.

[12] A.B. Djurisic, A.M.C.Ng, X.Y. Chen, ZnO nanostructures for optoelectronics: Material properties and device applications, Progress in Quantum Electronics 34 (2010) 191–259.

[13] C. Ye, X. Fang, Y. Hao, X. Teng, L. Zhang, Zinc Oxide Nanostructures: Morphology Derivation and Evolution, J. Phys. Chem. B 109 (2005) 19758-19765.

[14] Z.L. Wang, X.Y. Kong, Y. Ding, P. Gao, W.L. Hughes, R. Yang, Y. Zhang, Semiconducting and piezoelectric oxide nanostructure induced by polar surfaces, Adv. Funct. Mater. 14 (2004) 943-56.

[15] Z.L. Wang, Zinc oxide nanostructures: growth, properties and applications J. Phys.: Condens. Matter 16 (2004) R829-R858

[16] F. Giovannelli, G. Rajonson, J. Wolfman, F. Delorme, Synthesis of ZnO microwires and tetrapods by optical furnace, Materials Letters 107 (2013) 194–196

[17] J. Jolivet , S. Cassaignon, C. Chanéac, D. Chiche, O. Durupthy, D. Portehault, Design of metal oxide nanoparticles : control of size, shape, crystalline structure and functionalization by aqueous chemistry C. R. Chimie 13 (2010) 40–51.

[18] Baes CF, Mesmer RE, The hydrolysis of cations. Wiley and Sons, New York (1976) 112–123.

[19] F. Giovannelli, C. Autret-Lambert, C. Mathieu, T. Chartier, F. Delorme, A Seron, Synthesis of manganese spinel nanoparticles at room temperature by coprecipitation, Journal of Solid State Chemistry 192 (2012) 109–112

[20] D. Raoufi, Synthesis and microstructural properties of ZnO nanoparticles prepared by precipitation method, Renewable Energy 50 (2013) 932-937.

[21] A. Moezzi, A. McDonagh, A. Dowd, M. Cortie, Zinc hydroxyacetate and its transformation to nanocrystalline zinc oxide, Inorg. Chem. 52 (2013) 95-102.

[22] P. Chand, A. Gaur, A. Kumar, Structural and optical properties of ZnO nanoparticles synthesized at different pH values J. Alloys and Compounds 539 (2012) 174-178.

[23] K. Sambath, M. Saroja, M. Venkatachalam, K. Rajendran, N. Muthukumarasamy, Morphology controlled synthesis of ZnO nanostructures by varying pH, J. Mater. Sci : Mater Electron. 23 (2012) 431-436.

[24] R. Wahab, S.G. Ansari, H. Seo, Y. Kim, E. Suh, H. Shin, Low temperature synthesis and characterization of rosette-like nanostructures of ZnO using solution process, Solid State Sci. 11 (2009) 439-443

[25] J. E. Rodrıguez-Paez, A. C. Caballero, M. Villegas, C. Moure, P. Duran, and J. F. Fernandez, Controlled precipitation methods: formation mechanism of ZnO nanoparticles, J. Euro. Ceram. Soc., 21 (2001) 925–930.

[26] W. Jia, S. Dang,H. Liu, Z. Zhang, C. Yu, X. Liu, B. Xu, Evidence of the formation mechanism of ZnO in aqueous solution Mater. Let. 82 (2012) 99-101.

[27] R. Wahab, Y. Kim, H. Shin, Synthesis, characterization and effect of pH variation on zinc oxide nanostructures, Mater. Transactions 50 (2009) 2092-2097.

[28] A.P. Almeida de Oliveira, J.-F. Hochepied, F. Grillon, M.-H. Berger, Controlled precipitation of zinc oxide particles at room temperature, Chem. Mater. 15 (2003) 3202-3207.

[29] L. Yang, L. Xiang, Influence of mixing ways of reactants on ZnO morphology, J. Nanomater. (2013) ID 289616, 6p.

[30] Gratuze B, Blet-Lemarquand M and Barrandon JN, Mass spectrometry with laser sampling: A new tool to characterize archaeological materials. Journal of Radioanalytical and Nuclear Chemistry 247 (2001) 645–656.

[31] S. Aries, M. Motellica-Heino, R. Freydier, T. Grezes, M. Polvé, Direct determination of lead isotope ratios by laser ablation-inductively coupled plasma-quadrupole mass spectrometry in lake sediment sample, J. Geostandards and Geoanalysis 25(2001) 387–398.

[32] M. Motelica-Heino, O.F.X. Donard, Comparison of UV and IR Laser Ablation ICP/MS with Silicate Reference Materials and Implementation of Normalization Factors for Quantitative measurements, Geostandard Newsletter 25 (2001) 2.

[33] K. Shirouzu, T. Ohkusa, M. Hotta, N. Enomoto, and J. Hojo, distribution ans solubility limit of Al in Al2O3 doped ZnO sintered body, J. Ceram. Soc. Japan, 115 (2007) 254-258.

[34] H. Serier, M. Gaudon, M. Menetrier, Al-doped ZnO powdered materials: Al solubility limit and IR absorption properties, Solid State Science 11 (2009) 1192-1197.

[35] W. Nowacki, J. N. Silverman, Die kristallstruktur von zinkhydroxychlorid II, $Zn_5(OH)_8Cl_2 \cdot 1H_2O$, Zeitschrift fur Kristallographie 115 (1961) 21-51.

[36] W. Stählin, H. R. Oswald, The crystal structure of zinc hydroxide nitrate, $Zn_5(OH)_8(NO_3)_2.2H_2O$, Acta Cryst. B 26 (1970) 860-863.

[37] F. Delorme , A. Seron, Hydroxides : Synthesis, Types and Applications, A.C. Carillo and D.A. Griego (Ed.) (2012) 169-194.

[38] E. Hosono, S. Fujihara, T. Kimura, H. Imai, Non-basic solution routes to prepare ZnO nanoparticles, J. Sol-Gel and technology 29 (2004) 71-79.

[39] F. Caillaud, A. Smith, J.-F. Baumard, Effect of the solution on the deposition of zinc oxide films by spray pyrolysis, J. Am. Ceram. Soc. 76 (1993) 998–1002.

[40] P. Li, Z.P. Xu, M.A. Hampton, D.T. Vu, L. Huang, V. Rudolph, A.V. Nguyen, Control preparation of zinc hydroxide nitrate nanocrystals and examination of the chemical and structural stability, J. Phys. Chem. C 116 (2012) 10325-10332.

[41] S. Newman, W. Jones, Comparative study of some layered hydroxide salts containing exchangeable interlayer anions, J. Solid State Chem. 148 (1999) 26-40.

[42] F. Cavani, F. Trifiro, A. Vaccari, Hydrotalcite-type anionic clays: preparation, properties and applications, Catal. Today 11 (1991) 173-301.

[43] A. Seron, F. Delorme, Synthesis of layered double hydroxides (LDHs) with varying pH: A valuable contribution to the study of Mg/Al LDH formation mechanism, J. Phys. Chem. Solid 69 (2008) 1088–1090.

[44] J.W. Boclair, P.S. Braterman, Layered double hydroxide stability. 1. Relative stabilities of layered double hydroxides and their simple counterparts, Chem. Mater., 11 (1999) 298-302.

Figure captions

Figure 1: X-ray diffraction patterns of samples with different initial Zn concentrations.

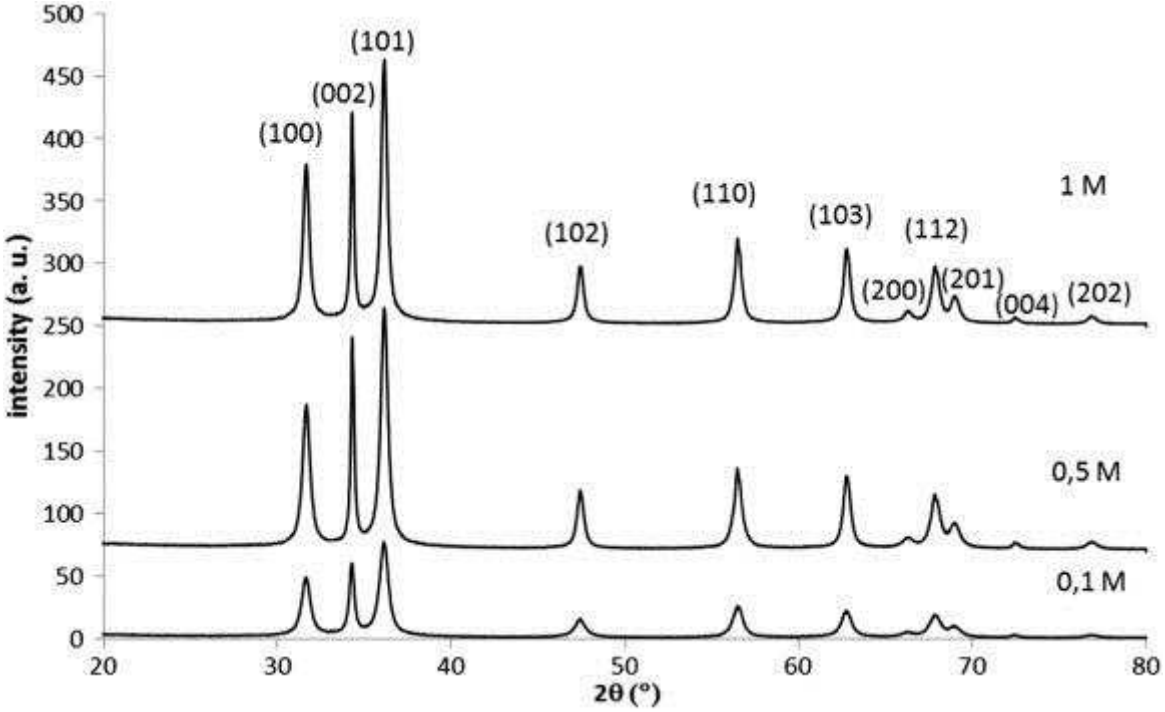

Figure 2: SEM images of samples with initial concentration of (A) 0.1M and (B) 1M.

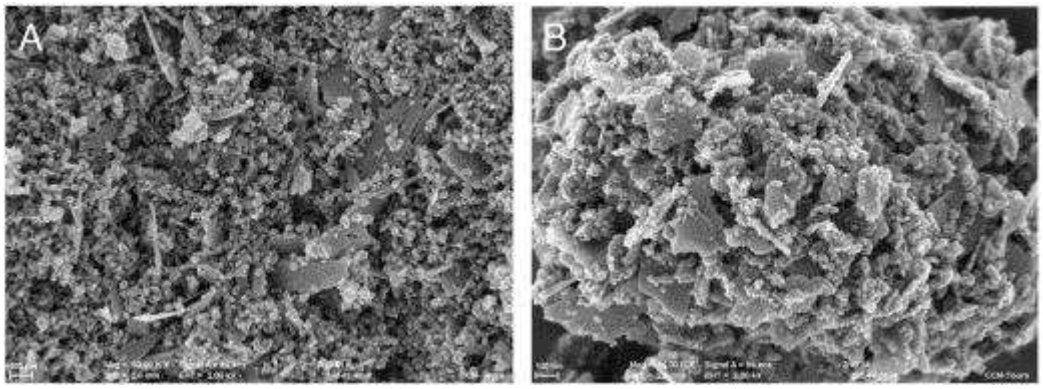

Figure 3: X-ray diffraction patterns of samples with different Zn/OH ratios

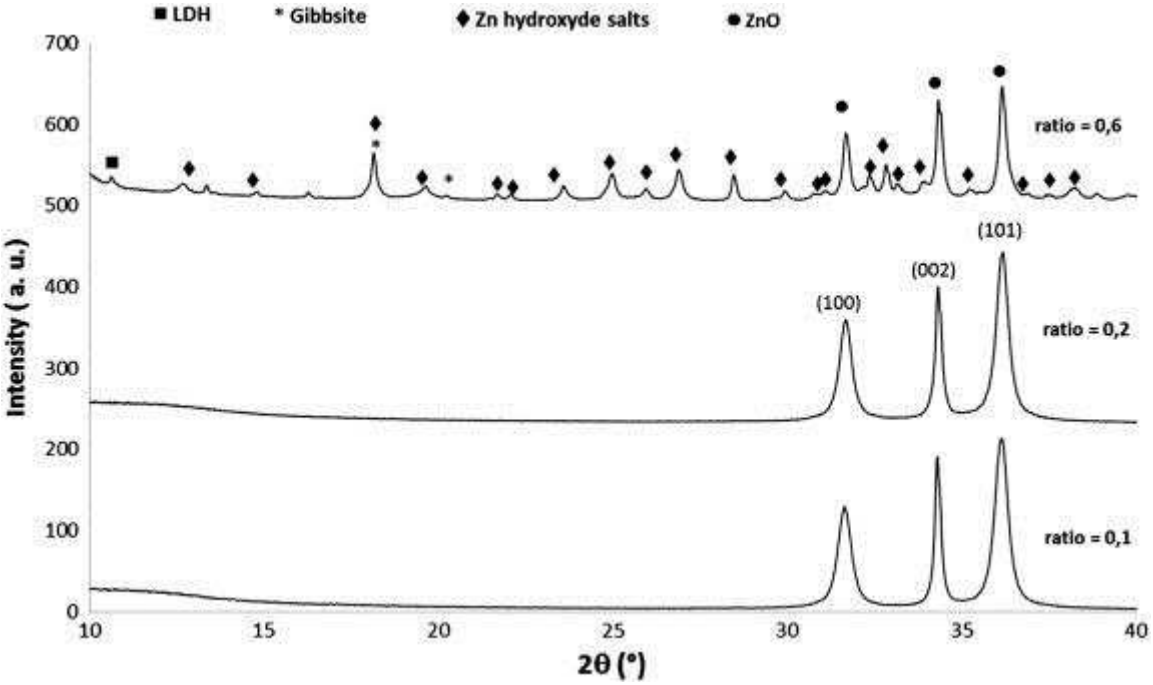

Figure 4: X-ray diffraction patterns of samples with (A) fast soda addition and (B) fast soda addition followed by 24h ageing.

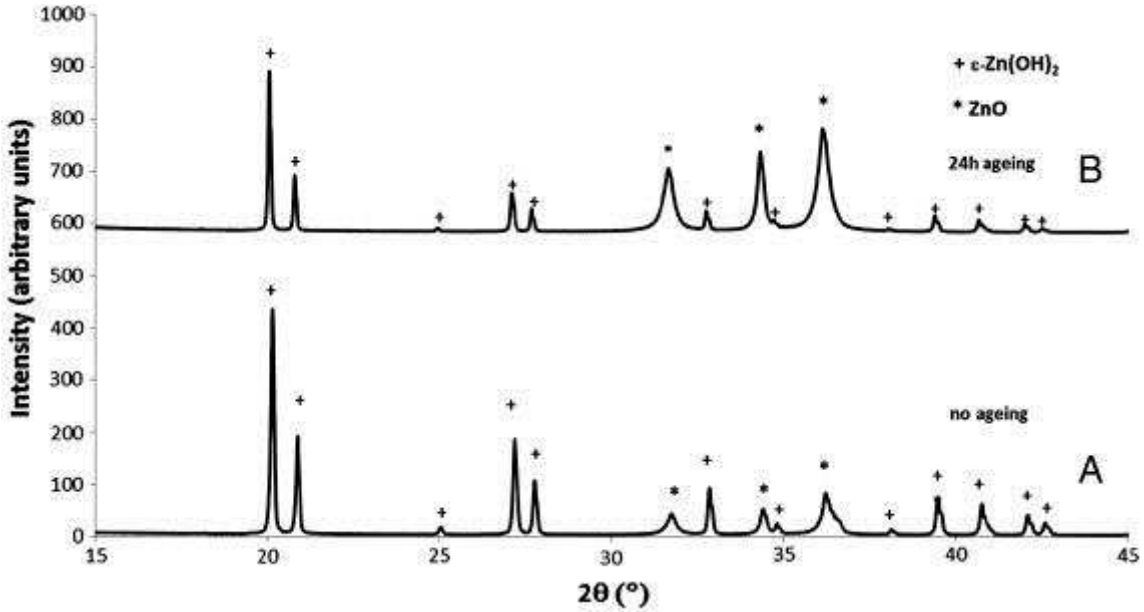

Figure 5: SEM images of obtained powders with (A) fast soda addition and (B) fast soda addition followed by 24h ageing.

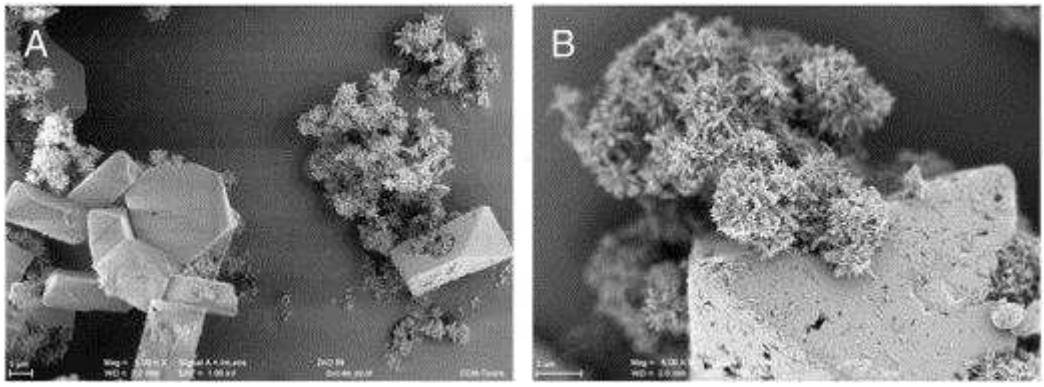

Figure 6: SEM images of (A) pure ZnO and (B) 5 at % Al doped ZnO.

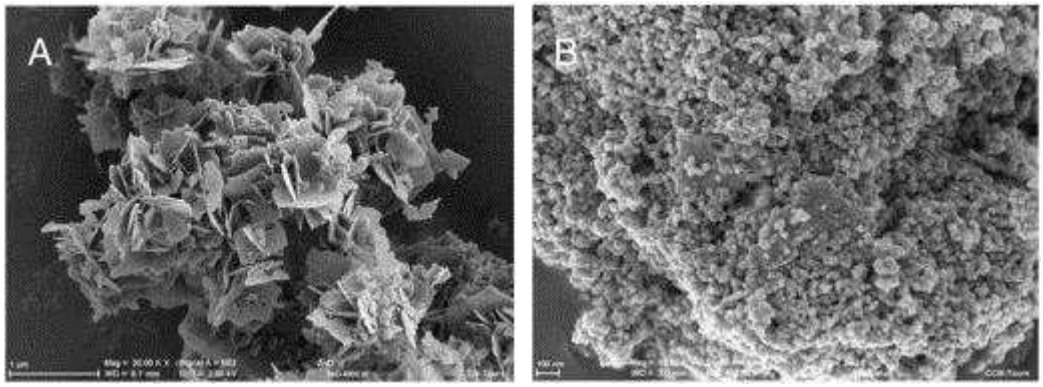

Figure 7: X-ray diffraction pattern of Al doped ZnO synthesized at 60°C.

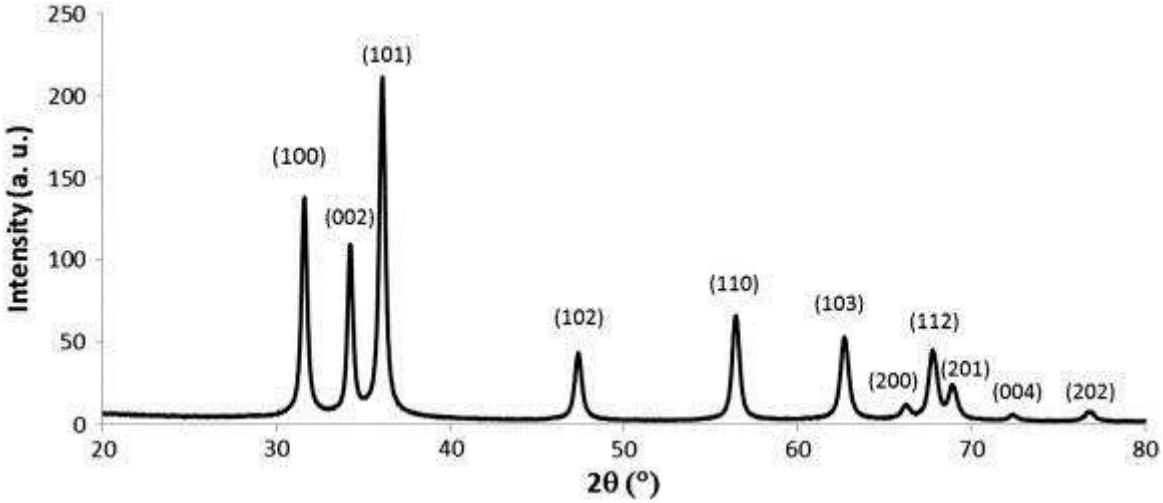

Figure 8: SEM image of Al doped ZnO synthesized at 60°C.